ELSEVIER

Chemical Engineering Science 62 (2007) 28–44

Chemical Engineering Science

www.elsevier.com/locate/ces

Review of discrete particle modeling of fluidized beds

N.G. Deen*, M. Van Sint Annaland, M.A. Van der Hoef, J.A.M. Kuipers

Faculty of Science and Technology, University of Twente, P.O. Box 217, 7500 AE Enschede, The Netherlands

Available online 22 August 2006

Abstract

This paper reviews the use of discrete particle models (DPMs) for the study of the flow phenomena prevailing in fluidized beds. DPMs describe the gas-phase as a continuum, whereas each of the individual particles is treated as a discrete entity. The DPMs accounts for the gas–particle and particle–particle interactions. This model is part of a multi-level modeling approach and has proven to be very useful to generate closure information required in more coarse-grained models. In this paper, a basic DPM, based on both the hard- and soft-sphere approaches is described. The importance of the closures for particle–particle and gas–particle interaction is demonstrated with several illustrative examples. Finally, an outlook for the use of DPMs for the investigation of various chemical engineering problems in the area of fluidization is given.

Keywords: Fluidization; Discrete particle model; Multi-scale modeling

1. Introduction

Fluidized beds are widely used in the chemical and process industries for a large variety of processes. In order to improve design and scale-up procedures of fluidized beds, a sound understanding of the transport phenomena in these systems is vital. There exists a vast amount of literature on various experimental investigations of transport phenomena in fluidized beds. Often, flat, pseudo-two-dimensional fluidized beds are used to study the fluidization behavior with the aid of video techniques or probe measurements because three-dimensional fluidized beds are not visually accessible. Although the latter system can be utilized in principle probes, they in general, at least locally, disturb the fluidization behavior and thereby influence the outcome of the measurement. To overcome these practical limitations detailed computer models have gained considerable attention since the early 1990s. With the use of computer models one is able to 'look' inside the fluidized bed without disturbing the flow-field. Furthermore, the use of the discrete particle model (DPM) enables the simultaneous 'measurement' of several properties, such as the gas and particle velocities, and the porosity, which is difficult if not impossible to achieve by direct experimentation. Provided that computer models possess sufficient predictive capabilities, they have the additional advantage over experiments that several design options and operation conditions can be tested with relative ease.

Despite these advantages, the construction of reliable models for large-scale gas–solid contactors is seriously hindered by the lack of understanding of the fundamentals of dense gas–particle flows. In particular, the phenomena which can be related both to the effective gas–particle interaction (drag forces), particle–particle interactions (collision forces), and particle–wall interaction, are not well understood. The prime difficulty here is the large separation of scales: the largest flow structures can be of the order of meters; yet these structures are directly influenced by details of the particle–particle and particle–gas interactions, which take place on the scale of millimeters, or even micrometers. To describe the hydrodynamics of both the gas and particle phase, continuum-(Eulerian) and discrete-(Lagrangian) type of models have been developed. To model gas–solid two-phase flows at different scales, one can choose appropriate combinations of the gas- and solid-phase models, provided that a four-way coupling is used either directly or effectively, depending on the scale of the simulation domain. The basic idea is that the smaller scale models, which take into account the various interactions (fluid–particle,

* Corresponding author. Tel.: +31 53 489 4138; fax: +31 53 489 2882.
E-mail address: N.G.Deen@utwente.nl (N.G. Deen).

0009-2509/$ - see front matter © 2006 Elsevier Ltd. All rights reserved.
doi:10.1016/j.ces.2006.08.014

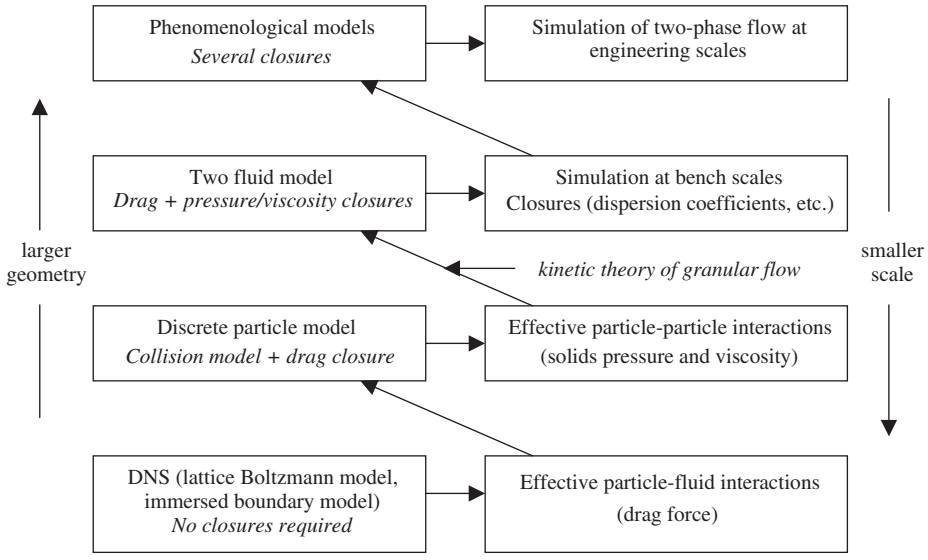

Fig. 1. Multi-level modeling scheme (after Van der Hoef et al., 2006).

particle–particle) in detail, are used to develop closure laws which can represent the effective 'coarse-grained' interactions in the larger scale models (Van der Hoef et al., 2004, 2005, 2006).

Note that in principle it is not guaranteed that all correlations between small- and large-scale processes can be captured by effective interactions. However, experience has shown that in many cases the main characteristics of gas–solid flows can be well described by the use of closure relations. In this paper we focus on the intermediate level of modeling: the DPM. Furthermore, its connection to the other two levels of modeling (i.e. the direct numerical simulations and the two-fluid model (TFM) or Euler–Euler model based on the kinetic theory of granular flow) will be highlighted. In Fig. 1 we show a schematic representation of the four models, including the information that is abstracted from the simulations, which is incorporated in higher scale models via closure relations, with the aid of experimental data or theoretical results.

Discrete element models or DPMs have been used for a wide range of applications involving particles (see, for example, the book of Ristow, 2000 and the references therein) ever since it was first proposed by Cundall and Strack (1979). A major difference with these traditional DPM models is that a detailed description of the gas-phase dynamics is required, in order to describe the interaction between the particles and the fluidizing air. The coupling of the DPM with a finite volume description of the gas-phase based on the Navier–Stokes equations was first reported in the open literature by Tsuji et al. (1993) and Hoomans et al. (1996) for the soft-sphere model and the hard-sphere model respectively. From this point we will refer to these Euler–Lagrange types of models (i.e. a discrete description of the particulate phase and a continuous description of the gas-phase) as DPMs (Fig. 2).

It is the purpose of this work to provide an overview of the development of discrete element models applied to fluidization since the work of Tsuji et al. (1993) and Hoomans et al. (1996) and to give an overview of the state of the art of these models today. This work is organized as follows. First, we will present the framework of the collision model for both hard- and soft-sphere approaches, followed by a discussion of their numerical implementation. Subsequently, the different particle–particle and gas–particle interactions will be discussed in more detail, followed by a discussion of selected examples of applications of the DPM. We will conclude with an outlook on possible future developments of DPM with application to fluidized beds.

2. Framework of the collision model

2.1. Hard-sphere approach

In a hard-sphere system the trajectories of the particles are determined by momentum-conserving binary collisions. The interactions between particles are assumed to be pair-wise additive and instantaneous. In the simulation, the collisions are processed one by one according to the order in which the events occur. For not too dense systems, the hard-sphere models are considerably faster than the soft-sphere models. Note that the possible occurrence of multiple collisions at the same instant cannot be accounted for.

Campbell and Brennen (1985) reported the first hard-sphere discrete particle simulation used to study granular systems. Since then, the hard-sphere models have been applied to study a wide range of complex granular systems. Hoomans et al. (1996) used the hard-sphere model, in combination with a CFD approach for the gas-phase conservation equations, to study gas–solid two-phase flows in gas-fluidized beds. By using this model, they studied the effect of particle–particle interaction on bubble formation (Hoomans et al., 1996) and the particle segregation induced by particle size differences and density differences (Hoomans et al., 2000). This model has been further used in connection with the kinetic theory of granular flow by Goldschmidt et al. (2001), high-pressure fluidization by Li and

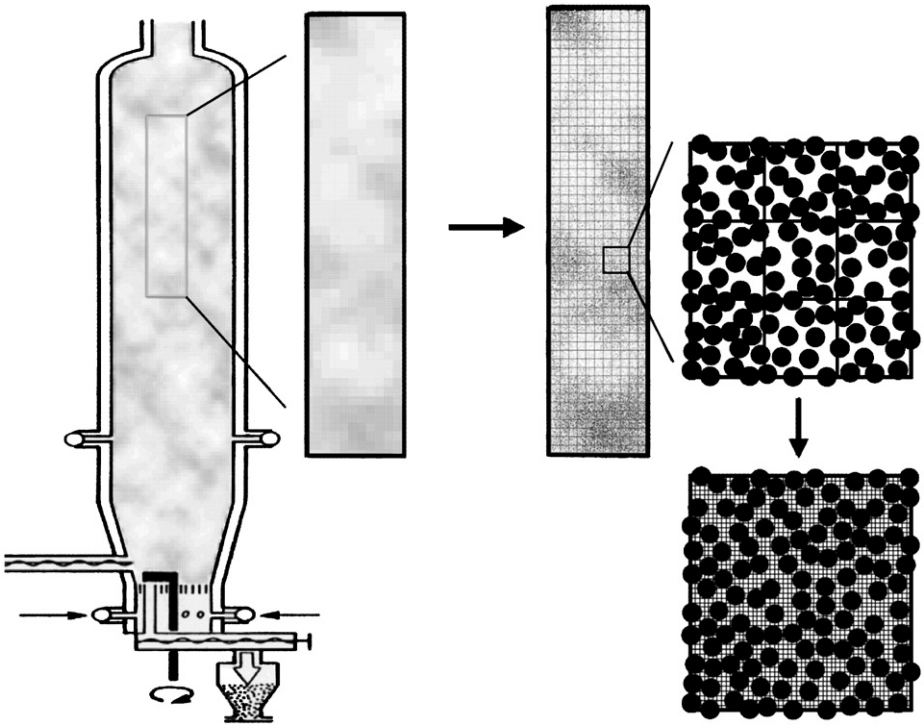

Fig. 2. Graphic representation of the multi-level modeling scheme. The arrows represent a change of model. On the left is a fluidized bed on a life-size scale that can be modeled with the aid of phenomenological models, a section of which is modeled by the two-fluid model (see enlargement), where the shade of gray of a cell indicates the solid phase volume fraction. On the right, the same section is modeled using discrete particles. The gas-phase is solved on the same grid as in the two-fluid model. The bottom graph shows the most detailed level, where the gas-phase is solved on a grid much smaller than the size of the particles (after Van der Hoef et al., 2006).

Kuipers (2002, 2003, 2005), circulating fluidized beds by He et al. (2006), spout-fluid beds by Link et al. (2004, 2005) and particle flows through contractions by Vreman et al. (2006).

Similar simulations have been carried out by other research groups. Dahl et al. (2004) and Dahl and Hrenya (2004, 2005) applied a hard-sphere model to study segregation in continuous size distributions. Ouyang and Li (1999a,b) developed a slightly different version of this model. Helland et al. (1999) developed a DPM in which hard-sphere collisions are assumed, but where a time-driven scheme (typically found in the soft-sphere model) is used to locate the collisional particle pair. Effect of the gas turbulence has also been taken into account in some hard-sphere models by Helland et al. (2000, 2002, 2005), Ibsen et al. (2004), Lun (2000) and Zhou et al. (2004).

At high particle number densities or low coefficients of normal restitution e, the collisions will lead to a dramatical decrease in kinetic energy. This is the so-called inelastic collapse McNamara and Young (1992), in which regime the collision frequencies diverge as relative velocities vanish. Clearly in that case, the hard-sphere method becomes useless.

2.2. Soft-sphere approach

In more complex situations, the particles may interact via short- or long-range forces, and the trajectories are determined by integrating the Newtonian equations of motion. The soft-sphere method originally developed by Cundall and Strack (1979) was the first granular dynamics simulation technique published in the open literature. Soft-sphere models use a fixed time step and consequently the particles are allowed to overlap slightly. The contact forces are subsequently calculated from the deformation history of the contact using a contact force scheme. The soft-sphere models allow for multiple particle overlap although the net contact force is obtained from the addition of all pair-wise interactions. The soft-sphere models are essentially time driven, where the time step should be carefully chosen in the calculation of the contact forces. The soft-sphere models that can be found in literature mainly differ from each other with respect to the contact force scheme that is used. A review of various popular schemes for repulsive inter-particle forces is presented by Schäfer et al. (1996). Walton and Braun (1986) developed a model which uses two different spring constants to model the energy dissipation in the normal and tangential direction respectively. In the force scheme proposed by Langston et al. (1994), a continuous potential of an exponential form is used, which contains two unknown parameters: the stiffness of the interaction and an interaction constant.

A two-dimensional soft-sphere approach was first applied to gas-fluidized beds by Tsuji et al. (1993), where the linear-spring/dashpot model similar to the one presented by Cundall and Strack (1979) was employed. Kawaguchi et al. (1998) extended this model to three dimensions as far as the motion

of the particles is concerned. Yu and co-workers (Xu and Yu, 1997; Xu et al., 2000; Yu and Xu, 2003) independently developed a two-dimensional model of a gas-fluidized bed. However, in their simulations a collision detection algorithm that is normally found in hard-sphere simulations was used to determine the first instant of contact precisely. Feng and Yu (2004) and Feng et al. (2004) applied this model to study segregation processes of a binary mixture.

Based on the model developed by Tsuji et al. (1993), Iwadate and Horio (1998) and Mikami et al. (1998) incorporated Van der Waals forces to simulate fluidization of cohesive particles. Further studies of the influence of gas and particle properties for Geldart A particles were performed by Ye et al. (2004, 2005b) and Pandit et al. (2005). Kafui et al. (2002) developed a DPM based on the theory of contact mechanics, thereby enabling the collision of the particles to be directly specified in terms of material properties such as friction, elasticity, elasto-plasticity and auto-adhesion. The soft-sphere model has been coupled to models describing mass transfer and chemical reactions to study the decomposition of ozone on catalyst coated particles in a two-dimensional fluidized bed by Limtrakul et al. (2004). Kuwagi et al. (2000) coupled the soft-sphere model with a model for the description of metallic solid bridging by surface diffusion mechanisms including the effect of surface roughness.

3. Governing equations

3.1. The discrete particles

The motion of every individual element i (particle or droplet) with mass m_i and volume V_i in the system is calculated from Newton's second law

$$m_i \frac{\mathrm{d}\mathbf{v}_i}{\mathrm{d}t} = m_i \frac{\mathrm{d}^2\mathbf{r}_i}{\mathrm{d}t^2} = -V_i \nabla p + \frac{V_i \beta}{\varepsilon_s}(\mathbf{u}_g - \mathbf{v}_i) + m_i \mathbf{g} + \mathbf{F}_{\mathrm{contact},i} + \mathbf{F}_{pp,i}, \quad (1)$$

where $\mathbf{v}_i$ is the velocity and $\mathbf{r}_i$ the position of the element i. The forces on the right-hand side of Eq. (1) are respectively due to the pressure gradient, drag, gravity, contact forces (i.e. due to collisions) and (long-range) particle–particle interaction (for instance Van der Waals forces):

The angular momentum of the particle is computed with

$$I_i \frac{\mathrm{d}\boldsymbol{\omega}_i}{\mathrm{d}t} = \mathbf{T}_i, \quad (2)$$

where T is the torque and I is the moment of inertia, which for spherical particles with radius R_i is equal to $I_i = \frac{2}{5} m_i R_i^2$.

The inter-phase momentum transfer coefficient β is frequently modelled by combining the Ergun (1952) equation for dense regimes ($\varepsilon_g < 0.8$)

$$F_{\mathrm{Ergun}} = \frac{\beta d_p^2}{\mu} = 150\frac{\varepsilon_s^2}{\varepsilon_g} + 1.75\varepsilon_s Re \quad (3)$$

and the correlation proposed by Wen and Yu (1966) for the more dilute regimes ($\varepsilon_g > 0.8$)

$$F_{\mathrm{Wen\ and\ Yu}} = \frac{\beta d_p^2}{\mu} = \frac{3}{4} C_D Re\, \varepsilon_s \varepsilon_g^{-2.65};$$
$$C_D = \begin{cases} 24(1 + 0.15Re^{0.687})/Re & \text{if } Re < 10^3, \\ 0.44 & \text{if } Re > 10^3, \end{cases} \quad (4)$$

where $Re = \varepsilon_g \rho_g |\mathbf{u}_g - \mathbf{v}_p| d_p/\mu_g$ is the particle Reynolds number and ε_g is the gas volume fraction ($\varepsilon_g = 1 - \varepsilon_s$). The particle Reynolds number is usually much larger than unity, which gives rise to an unrealistic jump in the drag curve at $\varepsilon_g = 0.8$. This problem can be circumvented by using the least value of Eqs. (3) and (4) for the calculation of β.

Hill et al. (2001) derived the following drag relation for $Re > 40$, obtained from simulations using the lattice Boltzmann approach:

$$F_{\mathrm{Hill}} = \frac{\beta d_p^2}{\mu} = A\frac{\varepsilon_s^2}{\varepsilon_g} + B\varepsilon_s Re$$
$$A = \begin{cases} 180, & \varepsilon_g < 0.6, \\ \dfrac{18\varepsilon_g^3}{\varepsilon_s} \dfrac{1 + \frac{3}{\sqrt{2}}\varepsilon_s^{1/2} + \frac{135}{64}\varepsilon_s \ln \varepsilon_s + 16.14\varepsilon_s}{1 + 0.681\varepsilon_s - 8.48\varepsilon_s^2 + 8.16\varepsilon_s^3}, & \varepsilon_g > 0.6, \end{cases}$$
$$B = 0.6057\varepsilon_g^2 + 1.908\varepsilon_s\varepsilon_g^2 + 0.209\varepsilon_g^{-3}. \quad (5)$$

Note that this expression for A is slightly different from the actual lattice Boltzmann data of Hill et al. (2001). For a discussion of on this point see the work of Benyahia et al. (2006) and Beetstra et al. (2006a).

Using a similar approach as Hill et al. (2001), Beetstra et al. (2006a) derived the following drag relation:

$$F_{\mathrm{Beetstra}} = \frac{\beta d_p^2}{\mu} = A\frac{\varepsilon_s^2}{\varepsilon_g} + B\varepsilon_s Re$$
$$A = 180 + \frac{18\varepsilon_g^4}{\varepsilon_s}\left(1 + 1.5\sqrt{\varepsilon_s}\right),$$
$$B = \frac{0.31(\varepsilon_g^{-1} + 3\varepsilon_g\varepsilon_s + 8.4Re^{-0.343})}{1 + 10^{3\varepsilon_s}Re^{2\varepsilon_g - 2.5}}. \quad (6)$$

The latter relation is based on a wider range of data than the expression of Hill et al. (2001), for Reynolds numbers up to 1000 showing proper limiting behavior and is therefore believed to be of more practical value than the correlation of Hill et al. (2001).

3.2. The gas-phase

The gas-phase hydrodynamics are calculated from the volume-averaged Navier–Stokes equations:

$$\frac{\partial}{\partial t}(\varepsilon_g \rho_g) + \nabla \cdot (\varepsilon_g \rho_g \mathbf{u}_g) = 0, \quad (7)$$

$$\frac{\partial}{\partial t}(\varepsilon_g \rho_g \mathbf{u}_g) + \nabla \cdot (\varepsilon_g \rho_g \mathbf{u}_g \mathbf{u}_g) = -\varepsilon_g \nabla p_g - \nabla \cdot (\varepsilon_g \boldsymbol{\tau}_g) - \mathbf{S}_p + \varepsilon_g \rho_g \mathbf{g}. \quad (8)$$

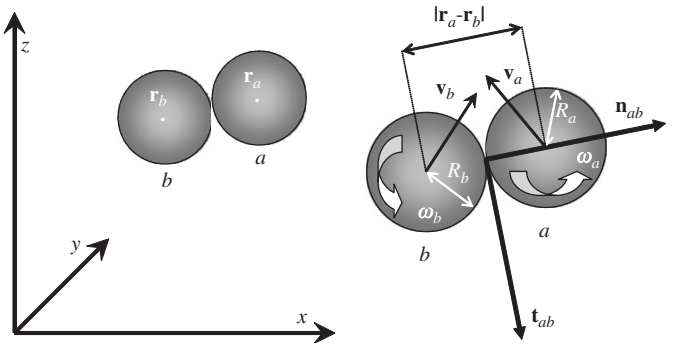

Fig. 3. The coordinate system used in the description of the discrete particle collision models.

The gas-phase stress tensor is given by

$$\boldsymbol{\tau}_g = -(\lambda_g - \tfrac{2}{3}\mu_g)(\nabla \cdot \mathbf{u}_g)\mathbf{I} - \mu_g((\nabla \mathbf{u}_g) + (\nabla \mathbf{u}_g)^{\mathrm{T}}), \tag{9}$$

where the bulk viscosity λ_g can be set to zero for gases. The two-way coupling between the gas-phase and the particles is enforced via the sink term $\mathbf{S}_p$ in the momentum equations of the gas-phase, which is computed from:

$$\mathbf{S}_p = \frac{1}{V_{\mathrm{cell}}} \int_{V_{\mathrm{cell}}} \sum_{i=0}^{N_p} \frac{V_i \beta}{\varepsilon_s} (\mathbf{u}_g - \mathbf{v}_i) D(\mathbf{r} - \mathbf{r}_i)\, \mathrm{d}V. \tag{10}$$

The distribution function D distributes the reaction force acting on the gas-phase to the Eulerian grid. When the volume of the smallest computational cell for the fluid is much larger than the volume of a particle, the mapping of properties from the Lagrangian particle positions to the Eulerian computational grid and vice versa can be done in a straightforward manner through volume-weighing techniques (Hoomans et al., 1996; Delnoij et al., 1999). On the other hand, when a high spatial resolution is required for the solution of the gas flow field, the computational grid can become smaller than the particle size. In that case, other distribution functions are needed, one of which is introduced in the section on numerical implementation.

3.3. Hard-sphere collision model

The collision model described in this work is based on the hard-sphere model developed by Hoomans et al. (1996, 2000, 2001). In this model it is assumed that the interaction forces are impulsive and therefore all other finite forces are negligible during a collision. Consider two colliding spheres a and b with position vectors $\mathbf{r}_a$ and $\mathbf{r}_b$ and radii R_a and R_b (see Fig. 3). The particle velocities prior-to-collision are indicated by the subscript 0 and the relative velocity at the contact point c is defined as follows:

$$\mathbf{v}_{ab} \equiv \mathbf{v}_{a,c} - \mathbf{v}_{b,c} = (\mathbf{v}_a - \mathbf{v}_b) - (R_a\boldsymbol{\omega}_a + R_b\boldsymbol{\omega}_b) \times \mathbf{n}_{ab}. \tag{11}$$

The normal and tangential unit vectors are respectively defined as:

$$\mathbf{n}_{ab} = \frac{\mathbf{r}_a - \mathbf{r}_b}{|\mathbf{r}_b - \mathbf{r}_a|} \quad \text{and} \quad \mathbf{t}_{ab} = \frac{\mathbf{v}_{ab,0} - \mathbf{n}_{ab} \cdot \mathbf{v}_{ab,0}}{|\mathbf{v}_{ab,0} - \mathbf{n}_{ab} \cdot \mathbf{v}_{ab,0}|}. \tag{12}$$

For a binary collision of these spheres, the following equations can be derived by applying Newton's second and third law:

$$m_a(\mathbf{v}_a - \mathbf{v}_{a,0}) = -m_b(\mathbf{v}_b - \mathbf{v}_{b,0}) = \mathbf{J}, \tag{13}$$

$$\frac{I_a}{R_a}(\boldsymbol{\omega}_a - \boldsymbol{\omega}_{a,0}) = -\frac{I_b}{R_b}(\boldsymbol{\omega}_b - \boldsymbol{\omega}_{b,0}) = -\mathbf{n}_{ab} \times \mathbf{J}. \tag{14}$$

Eqs. (13) and (14) can be rearranged to obtain:

$$\mathbf{v}_{ab} - \mathbf{v}_{ab,0} = \frac{7\mathbf{J} - 5\mathbf{n}_{ab}(\mathbf{J} \cdot \mathbf{n}_{ab})}{2m_{ab}}, \tag{15}$$

where m_{ab} is the reduced mass given by

$$m_{ab} = \left(\frac{1}{m_a} + \frac{1}{m_b}\right)^{-1}. \tag{16}$$

In order to calculate the post-collision velocities, a closure model consisting of three parameters is used to describe the impulse vector $\mathbf{J}$. The parameters are the coefficient of normal restitution ($0 \leqslant e_n \leqslant 1$),

$$\mathbf{v}_{ab} \cdot \mathbf{n}_{ab} = -e_n(\mathbf{v}_{ab,0} \cdot \mathbf{n}_{ab}), \tag{17}$$

the coefficient of dynamic friction ($\mu \geqslant 0$),

$$|\mathbf{n}_{ab} \times \mathbf{J}| = -\mu(\mathbf{n}_{ab} \cdot \mathbf{J}), \tag{18}$$

and the coefficient of tangential restitution ($0 \leqslant \beta_0 \leqslant 1$),

$$\mathbf{n}_{ab} \times \mathbf{v}_{ab} = -\beta_0(\mathbf{n}_{ab} \times \mathbf{v}_{ab,0}). \tag{19}$$

Combining Eqs. (15) and (17) yields the following expression for the normal component of the impulse vector:

$$J_n = -(1 + e_n)m_{ab}(\mathbf{v}_{ab,0} \cdot \mathbf{n}_{ab}). \tag{20}$$

For the tangential component, two types of collisions can be distinguished, i.e. sticking or sliding collisions. If the tangential component of the relative velocity is sufficiently high in comparison to the coefficients of friction and tangential restitution, gross sliding occurs throughout the whole duration of the contact and the collision is of the sliding type. The non-sliding collisions are of the sticking type. When β_0 is equal to zero, the tangential component of the relative velocity becomes zero during a sticking collision. When β_0 is greater than zero in such a collision, reversal of the tangential component of the relative velocity will occur. The criterion to determine the type of collision on basis of pre-collision information is as follows:

$$J_t = \begin{cases} -\frac{2}{7}(1+\beta_0) & \text{if } \mu J_n \geqslant \frac{2}{7}(1+\beta_0)m_{ab}(\mathbf{v}_{ab,0}\cdot\mathbf{t}_{ab}), \\ \quad \times m_{ab}(\mathbf{v}_{ab,0}\cdot\mathbf{t}_{ab}) & \\ -\mu J_n & \text{if } \mu J_n < \frac{2}{7}(1+\beta_0)m_{ab}(\mathbf{v}_{ab,0}\cdot\mathbf{t}_{ab}), \end{cases} \tag{21}$$

where the two equations describe collisions of the sticking and sliding type, respectively.

Given the definition of $\mathbf{J}$ in Eqs. (20) and (21), the post-collision velocities can now be calculated from Eqs. (13) and (14).

In particle–wall collisions the mass of particle b (i.e. the wall) is taken infinitely large, which makes all terms containing $1/m_b$ equal to zero, and consequently $m_{ab} = m_a$ in that case.

3.4. Soft-sphere collision model

In the soft-sphere model, the contact force on particle a is calculated as the sum of the contact forces of all particles in the contact list of particle a, i.e. all particles b, including walls, which are in contact with particle a:

$$\mathbf{F}_{\text{contact},a} = \sum_{\forall b \in \text{contactlist}} (\mathbf{F}_{ab,n} + \mathbf{F}_{ab,t}), \tag{22}$$

where $\mathbf{F}_{ab,n}$ and $\mathbf{F}_{ab,t}$ represent, respectively, the normal and tangential component of the contact force between particle a and b.

The torque only depends on the tangential contact force and is defined as follows:

$$\mathbf{T}_a = \sum_{\forall b \in \text{contactlist}} (R_a \mathbf{n}_{ab} \times \mathbf{F}_{ab,t}). \tag{23}$$

The calculation of the contact force between two particles is actually quite involved. A detailed model for accurately computing contact forces involves complicated contact mechanics (Johnson, 1985), the implementation of which is extremely cumbersome. Contact mechanics models can be simplified in order to reduce the calculation time, while maintaining sufficient accuracy in the energy household of the collisions. In this respect, many simplified models have been proposed, which use an approximate formulation of the inter-particle contact force. The simplest one is originally proposed by Cundall and Strack (1979), where a linear-spring and dashpot model is employed to calculate the contact forces.

In the latter model, the normal component of the contact force between two particles a and b can be calculated with

$$\mathbf{F}_{ab,n} = -k_n \delta_n \mathbf{n}_{ab} - \eta_n \mathbf{v}_{ab,n}, \tag{24}$$

where k_n is the normal spring stiffness, $\mathbf{n}_{ab}$ the normal unit vector, η_n the normal damping coefficient, and $\mathbf{v}_{ab,n}$ the normal relative velocity. The overlap δ_n is given by

$$\delta_n = R_a + R_b - |\mathbf{r}_b - \mathbf{r}_a|. \tag{25}$$

Using Eq. (12) for the relative velocity between particle a and b, the normal relative velocity is obtained as follows:

$$\mathbf{v}_{ab,n} = (\mathbf{v}_{ab} \cdot \mathbf{n}_{ab})\mathbf{n}_{ab}. \tag{26}$$

The normal damping coefficient is given by

$$\eta_n = \begin{cases} \dfrac{-2 \ln e_n \sqrt{m_{ab} k_n}}{\sqrt{\pi^2 + \ln^2 e_n}} & \text{if } e_n \neq 0, \\ 2\sqrt{m_{ab} k_n} & \text{if } e_n = 0, \end{cases} \tag{27}$$

where e_n is the coefficient of normal restitution, which has been defined in Eq. (17), and m_{ab} has been defined in Eq. (16). In particle–wall collisions the mass of particle b (i.e. the wall) is set infinitely large, resulting in $m_{ab} = m_a$.

For the tangential component of the contact force a Coulomb-type friction law is used

$$\mathbf{F}_{ab,t} = \begin{cases} -k_t \delta_t - \eta_t \mathbf{v}_{ab,t} & \text{if } |\mathbf{F}_{ab,t}| \leqslant \mu |\mathbf{F}_{ab,n}|, \\ -\mu |\mathbf{F}_{ab,n}| \mathbf{t}_{ab} & \text{if } |\mathbf{F}_{ab,t}| > \mu |\mathbf{F}_{ab,n}|, \end{cases} \tag{28}$$

where k_t, δ_t, η_t, and μ_f are the tangential spring stiffness, tangential displacement, tangential damping coefficient, and friction coefficient, respectively. The tangential relative velocity $\mathbf{v}_{ab,t}$ is defined as

$$\mathbf{v}_{ab,t} = \mathbf{v}_{ab} - \mathbf{v}_{ab,n}. \tag{29}$$

The tangential damping coefficient is defined as

$$\eta_t = \begin{cases} \dfrac{-2 \ln \beta_0 \sqrt{\frac{2}{7} m_{ab} k_t}}{\sqrt{\pi^2 + \ln^2 \beta_0}} & \text{if } \beta_0 \neq 0, \\ 2\sqrt{\frac{2}{7} m_{ab} k_t} & \text{if } \beta_0 = 0, \end{cases} \tag{30}$$

where β_0 is the friction coefficient, which has been defined in Eq. (19).

The tangential displacement is given by

$$\delta_t = \begin{cases} \delta_{t,0}\mathbf{H} + \int_{t_0}^{t} v_{ab,t}\, \mathrm{d}t & \text{if } |\mathbf{F}_{ab,t}| \leqslant \mu |\mathbf{F}_{ab,n}|, \\ \dfrac{\mu}{k_t} |\mathbf{F}_{ab,n}| \mathbf{t}_{ab} & \text{if } |\mathbf{F}_{ab,t}| > \mu |\mathbf{F}_{ab,n}|, \end{cases} \tag{31}$$

with

$$\mathbf{H} = \begin{bmatrix} qh_x^2 + c & qh_x h_y - sh_z & qh_x h_z + sh_y \\ qh_x h_y + sh_z & qh_y^2 + c & qh_y h_z - sh_x \\ qh_x h_z - sh_y & qh_y h_z + sh_x & qh_z^2 + c \end{bmatrix}, \tag{32}$$

where $\mathbf{h}$, c, s and q are defined as

$$\mathbf{h} = \frac{\mathbf{n}_{ab} \times \mathbf{n}_{0,ab}}{|\mathbf{n}_{ab} \times \mathbf{n}_{0,ab}|}, \quad c = \cos\varphi, \quad s = \sin\varphi, \quad q = 1 - c$$
$$\text{and} \quad \varphi = \arcsin(|\mathbf{n}_{ab} \times \mathbf{n}_{0,ab}|).$$

The required closures for the normal and tangential stiffness will be discussed in the section on interfacial interactions. For a more detailed discussion of this model we refer to Van der Hoef et al. (2006).

3.5. Inter-phase coupling

The equations for the gas-phase are coupled with those of the particle phase through the porosity and the inter-phase momentum exchange. All relevant quantities should be averaged over a volume, which is large compared to the size of the particles, and in such a way that they are independent of the Eulerian grid size.

A straightforward method for the calculation of the porosity was given by Hoomans et al. (1996). In their work, the porosity in an Eulerian cell is calculated as follows:

$$\varepsilon_{g,\text{cell}} = 1 - \frac{1}{V_{\text{cell}}} \sum_{\forall i \in \text{cell}} f_{\text{cell}}^{i} V_p^{i}, \tag{33}$$

where f_{cell}^{i} is the fractional volume of particle i residing in the cell under consideration. This method works well when the size of the grid cells is much larger than that of the particles (i.e. $V_{\text{cell}} \gg V_p$). From a numerical point of view, however, it is sometimes desirable to use small computational cells in

order to resolve all relevant details of the gas flow field and still obtain a grid-independent solution. Unfortunately, the method of Hoomans et al. (1996) generates problems once V_{cell} approaches V_p. That is, computational cells can be fully occupied by a particle, which leads to numerical problems. The calculation of the porosity and the two-way coupling between the gas-phase and the particles through the fluid–particle interaction requires the ratio between the size of the computational grid cells and the size of the particles to be large. To overcome these contradictory demands regarding the computational grid Link et al. (2005) developed an alternative inter-phase coupling method for the DPM.

In this method the porosity and the force exerted by the gas-phase on the particles are calculated in a grid-independent manner, thus allowing a sufficiently fine solution of the gas flow field. Link et al. (2005) represent the particles as porous cubes, where this geometry was selected because of its computational advantages. The diameter of the cube depends on the particle diameter and a constant scaling factor a, which defines the ratio between the cube and particle diameter and consequently the volume where interaction between the fluid and the particle under consideration occurs:

$$d_{\text{cube}} = a d_p. \tag{34}$$

The volume of the cube should be larger than or equal to the volume of the particle, resulting in:

$$a \geqslant \left(\frac{\pi}{6}\right)^{1/3} \approx 0.8. \tag{35}$$

In practice, a typically takes a value from 3 to 5. The porosity of a porous cube representing a particle is then equal to:

$$\varepsilon_{\text{cube}} = \frac{V_p}{V_{\text{cube}}} = \frac{\pi}{6a^3}. \tag{36}$$

Finally, the porous cube representation can be used to calculate the gas fraction in a computational cell in a manner analogous to Eq. (33)

$$\varepsilon_{g,\text{cell}} = 1 - \varepsilon_{\text{cube}} \sum_{\forall i \in \text{cell}} f^i_{\text{cell}}, \tag{37}$$

where f^i_{cell} is the volume fraction of the cell under consideration that is occupied by cube i. Contrary to the real particles, the cubes representing the particles are allowed to overlap.

By representing the particle as a porous cube, its presence is felt only relatively weakly in a larger portion of the flow domain. Consequently, grid refinement will not lead to local extremes in the gas fraction around the center of mass of the particle.

For the calculation of the drag force acting on the particle Link et al. (2005) uses a similar method. That is to say that a general variable ϕ_{cell} on the Eulerian grid can be mapped to a property ϕ_p on the Lagrangian position of the particle using the following equation:

$$\phi_p = \frac{1}{V_{\text{cube}}} \sum_{\forall j \in \text{cube}} f^{\text{cube}}_j V_j \phi_j, \tag{38}$$

where f^{cube}_j is the volume fraction of cell j occupied by the cube.

Vice versa, the backward mapping of a general variable ϕ_p on the Lagrangian particle position to a property on the Eulerian grid ϕ_{cell} can be done via

$$\phi_{\text{cell}} = V_{\text{cell}} \sum_{\forall i \in \text{cell}} \frac{f^i_{\text{cell}} \phi_i}{V_i}, \tag{39}$$

where f^i_{cell} is the volume fraction of the cell under consideration that is occupied by cube i. Link et al. (2005) demonstrated that the inter-phase coupling as described above yields grid independent results.

4. Numerical implementation

The computational strategy generally used for DPMs is displayed in Fig. 4. This figure shows a flow diagram of the different modules that constitute the model and the variables that are exchanged between the modules.

To resolve the time-dependent motion of the particles and the gas-phase, the DPM uses two different time scales. The main time step, δt_{flow}, is constant and is used to solve the Navier–Stokes equations and the inter-phase coupling. While for the particle–particle interaction a different time step is used, which depends on the particle–particle interaction approach.

In the soft-sphere approach a constant time step, δt_{soft}, is used to update the particle velocities, for instance by use of a

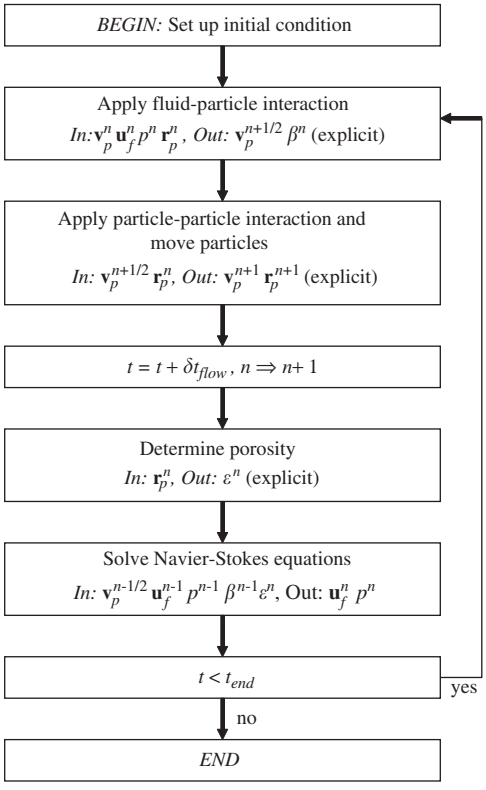

Fig. 4. Flow diagram of the discrete particle model.

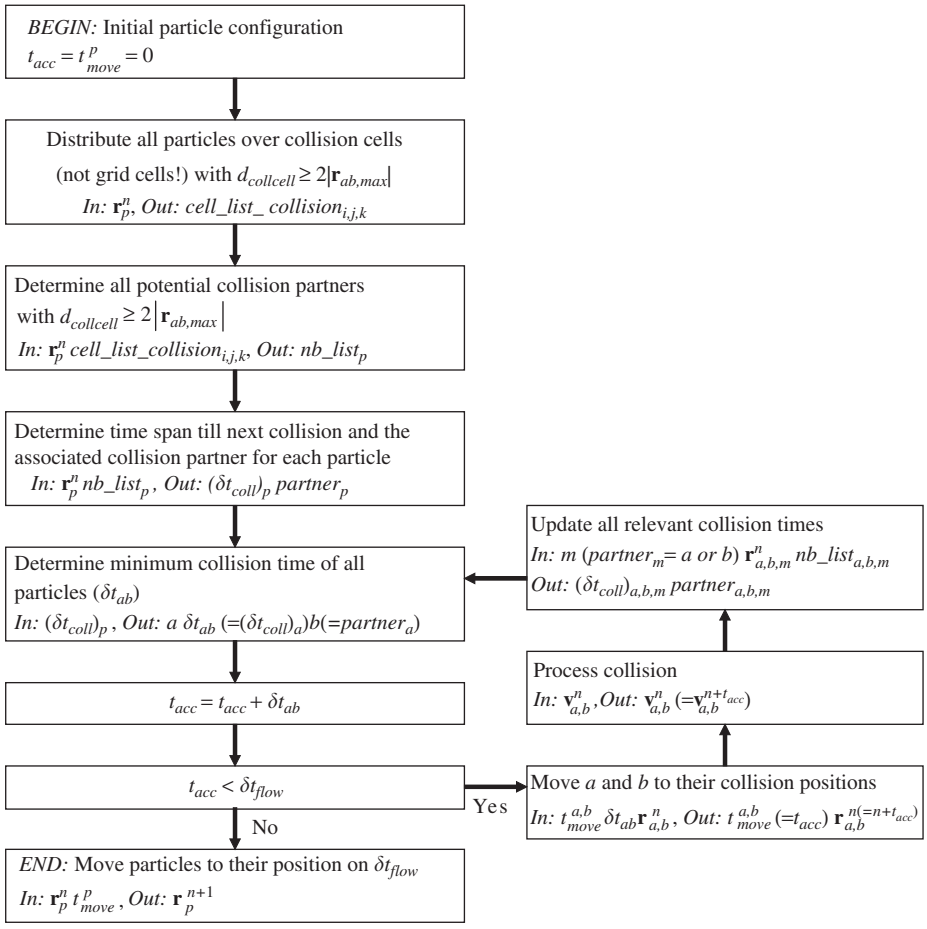

Fig. 5. Hard-sphere collision algorithm.

first order integration scheme for Newton's law

$$\mathbf{v}_i(t+\delta t_{\text{soft}}) = \mathbf{v}_i(t) + \frac{\mathbf{F}_i}{m_i}\delta t_{\text{soft}},$$
$$\mathbf{r}_i(t+\delta t_{\text{soft}}) = \mathbf{r}_i(t) + \mathbf{v}_i(t+\delta t_{\text{soft}})\delta t_{\text{soft}}, \quad (40)$$

with $\mathbf{F}_i(t)$ the total force on the RHS of Eq. (1) at time t. Note that this first-order scheme possesses very poor energy conservation, and for this reason it is advisable to use a higher-order scheme. More details can be found in Van der Hoef et al. (2006).

The time step should be sufficiently small to make sure that the contact lasts for a certain number of time steps to avoid problems concerning energy conservation due to the numerical integration, which is inevitable in the soft-sphere approach.

The contact time in the normal direction can be determined using

$$t_{\text{contact},n} = \sqrt{m_{ab}\frac{\pi^2 + \ln^2(e_n)}{k_n}}, \quad (41)$$

where m_{ab} is defined in Eq. (16) and e_n is defined in Eq. (17).

The contact time in the tangential direction can be determined using

$$t_{\text{contact},t} = \sqrt{\frac{2}{7}m_{ab}\frac{\pi^2 + \ln^2(\beta_0)}{k_t}}, \quad (42)$$

where β_0 is defined in Eq. (19).

To maintain the energy balance the normal and tangential contact times should be the same, which yields the following relation between k_t and k_n:

$$\frac{k_t}{k_n} = \frac{2}{7}\frac{\pi^2 + \ln^2(\beta_0)}{\pi^2 + \ln^2(e_n)}. \quad (43)$$

Although the normal stiffness can be determined from the Youngs modulus, it usually yields a very high value, which implies the use of a very small time step, which is undesirable from a computational point of view. In practice k_n is set to lower values, while ensuring that the normal overlap is kept small, i.e. typically below 1% of the particle diameter, ensuring that the predicted hydrodynamics are not affected.

The numerical implementation of the hard-sphere approach differs from that of the soft-sphere approach, in the sense that it is event driven, which means that the collision algorithm, illustrated in Fig. 5, is searching for the next collision in the fluidized

bed holding N_{part} particles with index $B=\{0, 1, \ldots, N_{\text{part}}-1\}$. In between subsequent collisions all particles are assumed to be in free flight.

To make the search for the next collision more efficient only collisions that can occur during one main time step δt_{flow} are considered. This limits the maximum distance $|\mathbf{r}_{ab}|_{\max}$ between particle a and potential collision partner b, which can also be a wall, to:

$$|\mathbf{r}_{ab}|_{\max} = R_a + R_{\max} + 2v_{\max}\delta t_{\text{flow}}, \tag{44}$$

where $R_{\max}=\max(R_a)\ \forall a \in B$ and $v_{\max}=\max(|\mathbf{v}_a|)\ \forall a \in B$.

All particles (including walls) within this distance of particle a make up its neighbor list, $Nb_{\text{list}}(a)$. The time required for a particle a to collide with a collision partner $b \in Nb_{\text{list}}(a)$ from their current position can be determined by

$$\delta t_{\text{pair}}(a,b) = \frac{-\mathbf{r}_{ab}\cdot\mathbf{v}_{ab} - \sqrt{(\mathbf{r}_{ab}\cdot\mathbf{v}_{ab})^2 - \mathbf{v}_{ab}^2(-\mathbf{r}_{ab}^2 - (R_a+R_b)^2)}}{\mathbf{v}_{ab}^2}, \tag{45}$$

where $\mathbf{r}_{ab} = \mathbf{r}_a - \mathbf{r}_b$. Note that if $\mathbf{r}_{ab}\cdot\mathbf{v}_{ab} > 0$ the particles are moving away from each other. In this case no collision is possible and $\delta t_{\text{pair}}(a,b)$ is discarded. The minimum of all $\delta t_{\text{pair}}(a,b)$ of particle a with partner $b \in Nb_{\text{list}}(a)$ is defined as the collision time of particle a:

$$\delta t_{\text{coll}}(a) = \min(\delta t_{\text{pair}}(a,b)) \quad \forall b \in Nb_{\text{list}}(a). \tag{46}$$

The time to the next collision in the entire calculation domain is obtained by

$$\delta t_{ab} = \min(\delta t_{\text{coll}}(a)) \quad \forall a \in B. \tag{47}$$

Subsequently, this time step is added to the time at which the last collision occurred:

$$t_{\text{acc}} = t_{\text{acc}} + \delta t_{ab}. \tag{48}$$

Only particle a and its partner b are moved to their new positions at time t_{acc} to minimize the number of computations (and accompanying accumulation of computational errors). This can only be done when the time each particle has moved within the timestep, t_{move} (which is taken into account for each subsequent calculation involving that particle) is stored.

Once the next collision is determined, momentum is exchanged between particle a and b, as described in the previous section. Subsequently only the collision times, δt_{coll} affected by the collision are updated, i.e. the collision times of the colliding particles themselves and of the particles that prior to the collision regarded one of the colliding particles as their collision partner. Once all collisions are processed ($t_{\text{acc}} > \delta t_{\text{flow}}$), all particles are moved to their position at δt_{flow}.

5. Discussion of interfacial interactions

5.1. Particle–particle interaction

It is well known that the formation of heterogeneous structures in fluidized beds can be attributed to a combination of the inelasticity of the particles and the strong non-linear dependency of the drag force on the porosity (Li and Kuipers, 2005). Hoomans et al. (1996) were among the first to investigate the effect of the particle collision properties on the fluidization behavior. They found that even for slightly inelastic particles, the dissipation of energy resulting from particle–particle collisions can give rise to heterogeneous structures. Due to the loss of energy during the collisions, the involved particles tend to cluster, forming dense regions next to dilute regions (i.e. bubbles).

These observations were confirmed by studies of Goldschmidt et al. (2002) who tested several particle properties for both the DPM and the TFM. They used the collision parameters that were determined from detailed impact measurements performed by the Impact Research Group of the Open University at Milton Keynes, where an accurate technique to measure collision parameters has been developed (Kharaz et al., 1999) and compared those to experimental data. They found a good correspondence between the numerical and experimental results, especially for the DPM. It is noted that in the case of wet particles, which are commonly found in several fluidized bed processes, such as spray granulation, the elasticity of the particles can be strongly reduced. This was shown by Fu et al. (2004), who investigated the change of the restitution coefficient as a function of the liquid-to-solid mass ratio for several wet particles. They found that for liquid-to-solid mass ratios larger than 0.2 particles become fully inelastic (i.e. the normal restitution coefficient approaches zero).

As mentioned earlier, it is usually assumed that particle–particle collisions are impulsive events that do not depend on the local flow field of the continuous phase. This assumption is only true in case the inertia of the continuous phase is negligible compared to that of the dispersed phase, which is the case for most of the contributions discussed in this work, in which the continuous phase is a gas. However, Zhang et al. (1999) have shown that the collision models as presented in the previous section need to be adapted when the continuous phase is a liquid, in order to account for the drainage of the fluid between the colliding particles and the acceleration of the fluid surrounding the particles. The adaptations of the DPM as proposed by Zhang et al. (1999) involve two additional forces, i.e. the virtual or added mass force and the pressure force. When these two forces are incorporated, the strong influence of the liquid surrounding the particles on the particle trajectories before and after the collision can be faithfully captured, as shown in Fig. 6. The closures for the close-distance interaction proposed by Zhang et al. (1999) were successfully used by Li et al. (1999, 2001) and Zhang et al. (2000a,b) in the two-dimensional VOF-DPM model for the hydrodynamic description of the particulate phase in a three-phase gas–liquid–solid flow. An extension of this approach to three dimensions was given by Chen and Fan (2004) who used a level-set method for the description of a large bubble and a DPM for the description of the particles. A similar model was reported by Van Sint Annaland et al. (2005) who combined a front tracking model with a DPM to describe the transport of particles in the wake of a single bubble rising in a liquid.

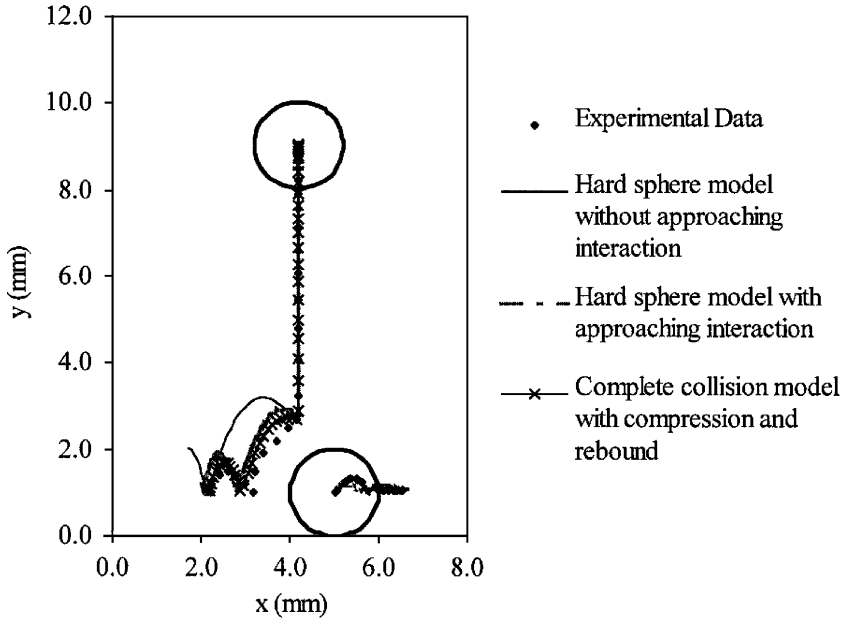

Fig. 6. Experimental and simulation results of trajectories of two colliding particles (taken from Zhang et al., 1999).

The virtual mass force was also considered in the work of Potic et al. (2005), who investigated fluidization behavior of hot compressed water in micro-reactors. They compared measured values of the minimum fluidization and minimum bubbling velocities with predictions of dedicated 2D and 3D DPM and (semi)-empirical relations. They found a good agreement between the measurements and the model predictions and concluded that the model supports the concept and development of micro-fluidized beds.

5.2. Gas–particle interaction

Various investigations of the closure relations for the drag force in the framework of continuum models have demonstrated that the choice of the drag closure has a significant impact on the resulting flow phenomena (see for instance Van Wachem et al., 2001; Ibsen, 2002; Andrews et al., 2005; Beetstra et al., 2006a). As indicated earlier, continuum models need closure models for both the drag force and the rheological properties of the particulate phase. One can only faithfully validate closure models for the drag force if and only if the rheological properties of the particulate phase are accurately known. Given the current limitations in the predictive capabilities of the TFM employing the kinetic theory of granular flow (Bokkers, 2005), it is much more worthwhile to use the DPM to validate closure models for the drag force since this model does not require closures for the rheological properties of the particles, which could give rise to anomalous behavior.

Link et al. (2005) has tested several drag closures in the DPM to assess their suitability to describe the particle dynamics in a pseudo-two-dimensional spout-fluid bed and compared the results with detailed particle image velocimetry measurement data. They compared time-averaged particle flux profiles and pressure drop fluctuations at different operating regimes for the following drag closures:

- The most frequently used drag model in literature, i.e.: the Ergun equation (3) for $\varepsilon_g < 0.8$, and the Wen and Yu equation (4) for $\varepsilon_g < 0.8$.
- The least value of the Eqs. (3) and (4), i.e. $F = \min(F_{\text{Ergun}}, F_{\text{Wen and Yu}})$.
- The drag relation derived from lattice Boltzmann simulations by Hill et al. (2001), i.e. Eq. (5).

As can be seen in Fig. 7, the first model produces unsatisfactory results for the shape of the vertical particle flux profiles $\Phi_{p,z}$ for fluidized beds with stable high-velocity jets, as encountered in spout-fluid beds. The usage of the minimum of the drag given by the relations of Ergun (1952), and Wen and Yu (1966), as well as the relation proposed by Hill et al. (2001) considerably improves the predictions of the DPM, although Link et al. (2005) found that the computed frequency of the pressure drop fluctuations is still somewhat too high. Li and Kuipers (2003) also investigated several drag relations for the case of a bubbling fluidized bed. They arrived at the same conclusion as Link et al. (2005), i.e. that the relation of Hill et al. (2001) has the best predictive capabilities. The expression recently proposed by Beetstra et al. (2006a) derived from similar type of LBM simulations is consistent with that of Hill et al. (2001), in particular when compared to the large deviations with the Ergun and Wen and Yu equations. For this reason, we expect that the simulation results as found by Li and Kuipers (2003) and Link et al. (2005) using the Hill et al. correlation will not be very different from the results that would be obtained with Eq. (6).

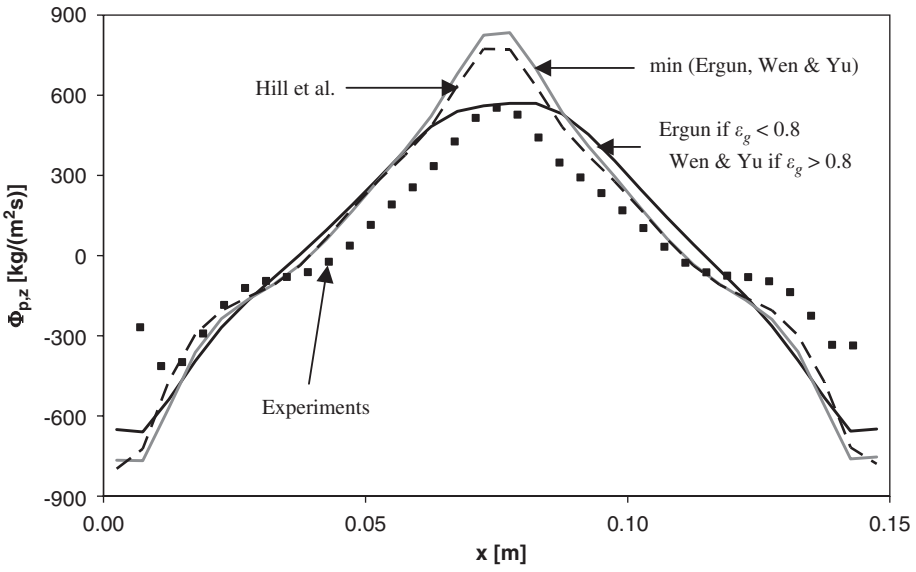

Spout-fluidization, $U_{fluidization} = 1.2 \times U_{mf}$, $U_{spout} = 23 \times U_{mf}$

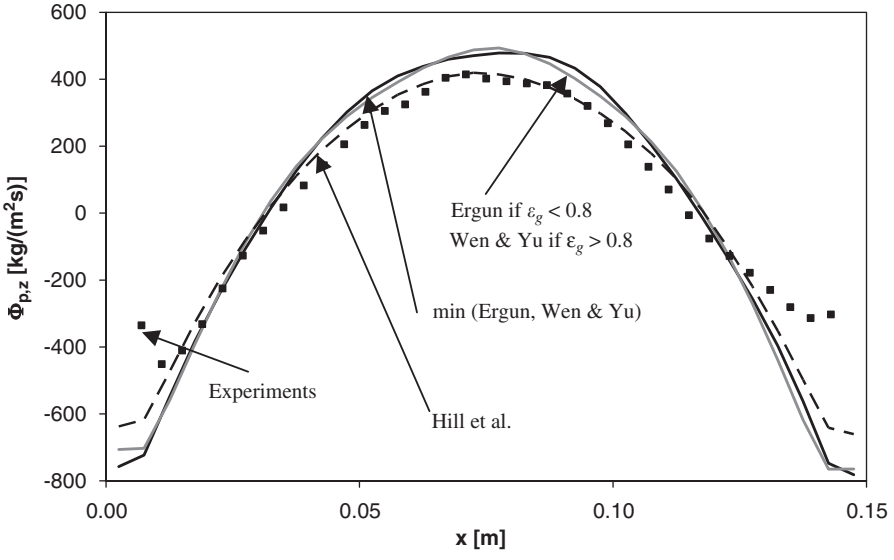

Jet in fluidized bed, $U_{fluidization} = 2.3 \times U_{mf}$, $U_{spout} = 16 \times U_{mf}$

Fig. 7. Measured and computed vertical time-averaged particle flux profiles for two different regimes using several drag closures (taken from Link et al., 2005).

6. Applications

6.1. Flow phenomena in fluidized beds

In this section we will discuss some of the recent applications of the DPM in the framework of research on the flow phenomena prevailing in fluidized beds. Many of the unique properties of gas-fluidized beds can be directly related to the gas bubbles behavior and therefore it is of crucial importance to assess the capability of the Euler–Lagrange model (DPM) to predict bubble formation and propagation in dense beds. Bokkers et al. (2004) studied the evolution of the bubble size and shape in time of a single bubble injected with a central jet into a fluidized bed, kept at minimum fluidization conditions via a porous plate distributor, with the use of a high-speed digital camera. Experiments were performed in a flat bed (0.30 m × 0.015 m × 1.00 m; 0.015 m jet width), with spherical glass beads of 2.5 mm diameter, fluidized with air. The initial bed height was 0.22 m, the background velocity was set at 1.25 m/s and the jet velocity and pulse duration were 20 m/s and 150 ms. Further details about the experimental setup can be found in Bokkers et al. (2004). In Fig. 8 snapshots of the bed at different moments in time after bubble injection are presented and compared with simulation results obtained with the DPM using a 40 × 80 grid (handling the particle dynamics fully 3D, while approximating the gas-phase as 2D). For the purpose of reference, the

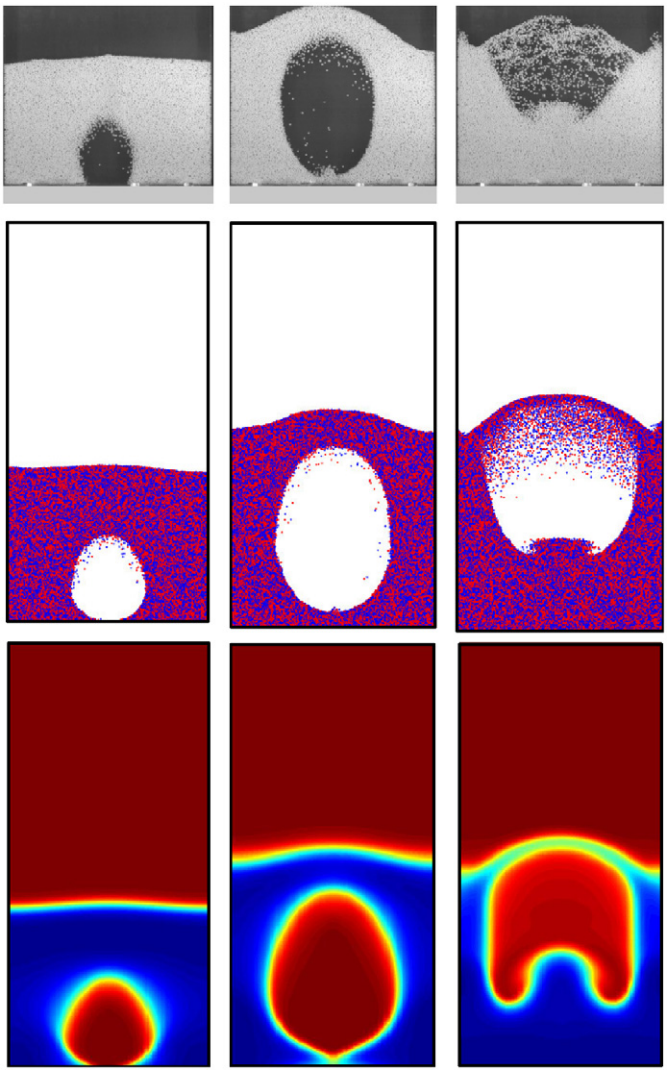

Fig. 8. Injection of a single bubble into the center of a mono-disperse fluidized bed (bed width: 0.30 m), consisting of spherical glass beads of 2.5 mm diameter at incipient fluidization conditions. Comparison of experimental data (top) with DPM (center) and TFM (bottom) simulation results for 0.1, 0.2, and 0.4 s after bubble injection (taken from Bokkers, 2005).

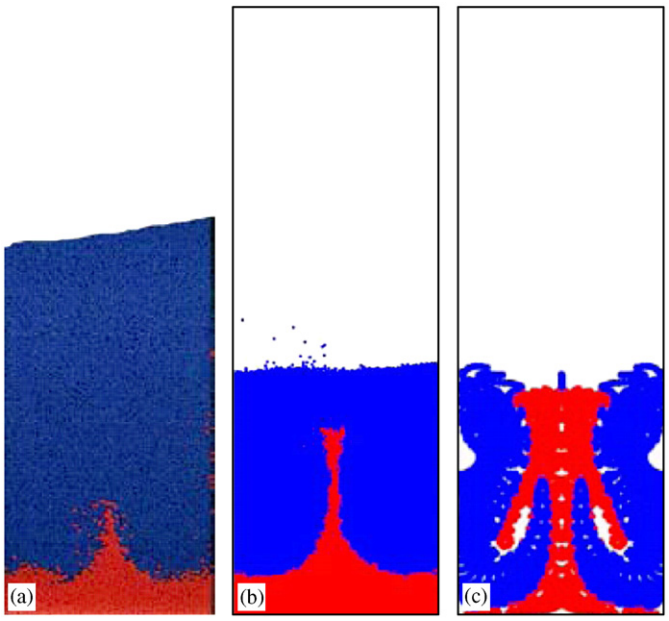

Fig. 9. Mixing patterns of a colored under-layer of particles ($d_p = 2.5$ mm) induced by a single bubble: (a) experiment; (b) discrete particle model (c) two-fluid model.

results of a TFM based on the kinetic theory of granular flow (Goldschmidt et al., 2004) using a 60×120 grid, employing a time step of 10^{-5} s are included. The restitution coefficient for particle–particle collisions was 0.97.

Both models capture the interaction of the particles with the jet: particles in the wake of the bubble are dragged into the center of the bubble, although this effect seems to be slightly overestimated by the TFM. Additionally, the raining of the particles through the roof of the bubble is predicted by the simulations. Both the DPM and TFM predict a slightly larger bubble size compared to the experiments for both beds, which can be attributed to the implemented equations for gas–particle drag (Ergun, 1952; Wen and Yu, 1966, drag closures). A somewhat better correspondence with experiments was obtained (see Bokkers et al., 2004) with new gas–particle drag closures derived from Lattice–Boltzmann simulations (Hill et al., 2001; Van der Hoef et al., 2005). Similar results were obtained for systems with different particle diameters and fluidization velocities. Concluding, the bubble size and shape for a single bubble injected into a bed at minimum fluidization conditions can be well described with the DPM and TFM, which provides a good basis to apply the DPM to more complex situations. The differences between the DPM and the TFM can best be observed from Fig. 9, which shows the particle mixing patterns induced by the passage of a single bubble through two initially completely segregated layers of particles of different color. The DPM shows good correspondence with the experimental observations, whereas the TFM largely overpredicts the mixing. This is caused by the fact that the KTGF only accounts for binary collisions between two particles, where friction between the particles is not included. Omitting friction between the particles and the corresponding additional dissipation of granular energy might result in an under-prediction of the shear viscosity of the solids phase.

Rhodes and co-workers (i.e. Rhodes et al., 2001a,b; Wang and Rhodes, 2003, 2004a,b, 2005a–c; Pandit et al., 2005; Takeuchi et al., 2004, 2005) used DPM simulations to study various aspects of fluidization, including the effect of cohesive forces on defluidization and particle mixing. Recently Wang and Rhodes (2005c) investigated the characteristics of pulsed fluidization with the aid of a two-dimensional soft-sphere model. They incorporated a periodically fluctuating component in the gas supply of a fluidized bed, which leads to two distinctive effects: ordered pressure fluctuations and regular bubble patterns. It was found that transition from chaotic to ordered behavior occurs as long as the applied frequency is not too low (e.g. 2 Hz). Formation of regular bubble patterns arises from periodical formation of a horizontal channel-like

structure near the distributor plate. Applied pulsation frequencies in a medium range, e.g. from about 5 to 15 Hz, give rise to regular bubble patterns. Increase in the amplitude of pulsation from about 0.125 to 1 × the minimum fluidization velocity was found to favor regulation of bubble patterns.

6.2. Generation of closures for continuum models (KTGF)

The mixing patterns predicted by the TFM presented in the previous section, illustrates that the TFM suffers from uncertainties in the closures, i.e. the kinetic theory of granular flow. One of the great advantages of discrete particle simulations is that it allows studying rheological properties of the system that are very difficult to obtain via experimentation. The velocity distribution of the particles is a particularly important example of a property that is difficult to acquire experimentally. It would be extremely difficult to obtain reliable estimates for the velocity distribution from experiments; yet, this function is of great relevance for the validity of higher scale models in the multi-level strategy, i.e. the TFM derived from the kinetic theory, where it is assumed that the velocity distribution is both isotropic and nearly Gaussian. The DPM is an ideal tool for testing this assumption, since it is relatively straightforward to measure the velocity distribution as all particle velocities are known at any moment in time. Goldschmidt et al. (2002) and Lu et al. (2005) both used the DPM to study the velocity distribution for the case of elastic and inelastic particles. Fig. 10 shows the results obtained by Goldschmidt et al. (2002) for a fluidized bed of ideal (i.e. perfectly smooth and elastic) and non-ideal (i.e. rough and inelastic) particles. The system contained 25,000 particles of 2.5 mm diameter, where the gas velocity is set to 1.5 times the minimum fluidization velocity. Details of the sampling procedure for obtaining the velocity distributions can be found in Goldschmidt et al. (2002). Fig. 10 shows that for both ideal and non-ideal particles, the velocity distributions do not deviate significantly from a Gaussian and Maxwellian distribution. However, Fig. 10 reveals a clear anisotropy of the distribution in case of non-ideal particles. A possible explanation is the formation of dense particle clusters in the case of inelastic collisions, which may disturb the spatial homogeneity and thereby causing collisional anisotropy. Analysis (Jenkins and Savage, 1983) of the normal and tangential component of the impact velocity indeed showed that, in dense gas-fluidized beds, not all impact angles occur with the same frequency.

Another example of the use of the DPM to generate closures for the two-fluid model is given in the work of Ye et al. (2005a), who used a soft-sphere DPM to test the kinetic theory, with an emphasis on the excess compressibility as it is the key quantity in KTGF for calculating the particle pressure and other transport coefficients. For slightly cohesive particles, only a very small deviation has been found from the classical kinetic theory of granular flows, which suggests that with the Hamaker constants tested in the range used in their research the cohesion only has a weak influence on the excess compressibility. It is expected that in the presence of a strong cohesive force, particles will form complicated agglomerates. In this case, an

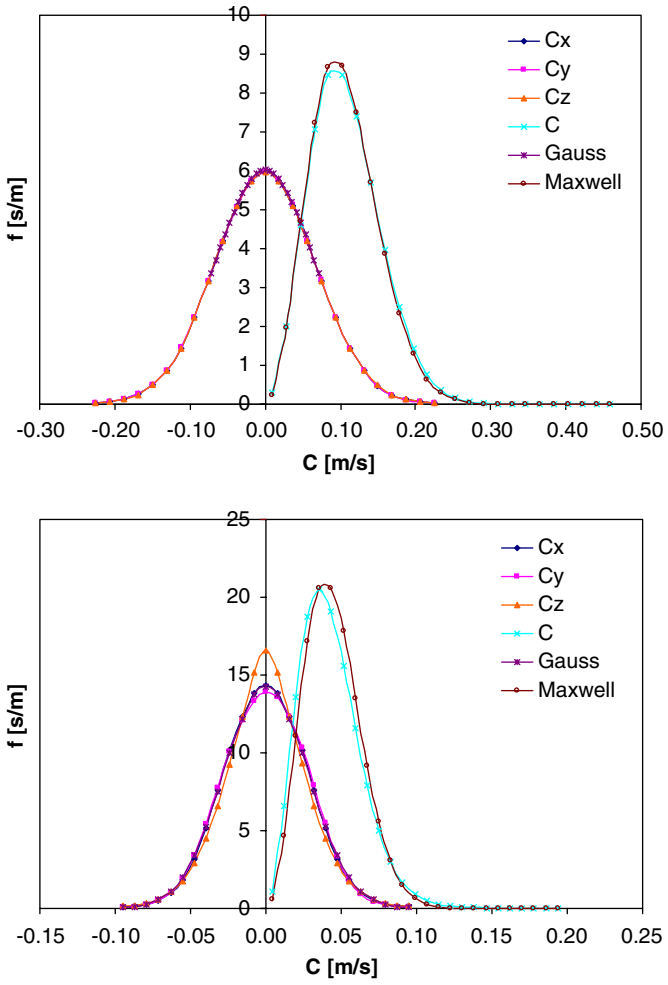

Fig. 10. DPM simulation data for the normalized particle velocity distribution $f_x(C_x)$, $f_y(C_y)$, $f_z(C_z)$ and $f(C)$, compared to a Gaussian/Maxwellian distribution. Top graph: ideal particles; bottom graph: non-ideal particles (taken from Goldschmidt et al., 2002).

equilibrium state may not exist, so that the validity of kinetic theory of granular flows is questionable. However, the quantification of the cohesive force is not straightforward, since there is no reference force (such as gravitational force) in these systems. Note also that the absolute value of the force is not precisely known, since it is extremely difficult to directly measure the cohesive forces between Geldart A particles, and a theoretical estimate based on the (bulk) particle properties is also unreliable since these forces strongly depend on the surface properties.

Another example is the simulation results of segregation in a *bidisperse* fluidized bed. Recently a new drag force relation for polydisperse systems has been suggested on the basis of lattice Boltzmann simulations (Beetstra et al., 2006b), and the DPM offers a way to test these relations, by comparing the segregation rate of a freely bubbling bed directly with experiments. These experiments were performed by Goldschmidt et al. (2003a) in which glass particles with diameters of 1.5 and 2.5 mm were fluidized with air in a pseudo-two-dimensional column of 15 × 45 × 1.5 ($H \times W \times D$) cm^3. The mixture

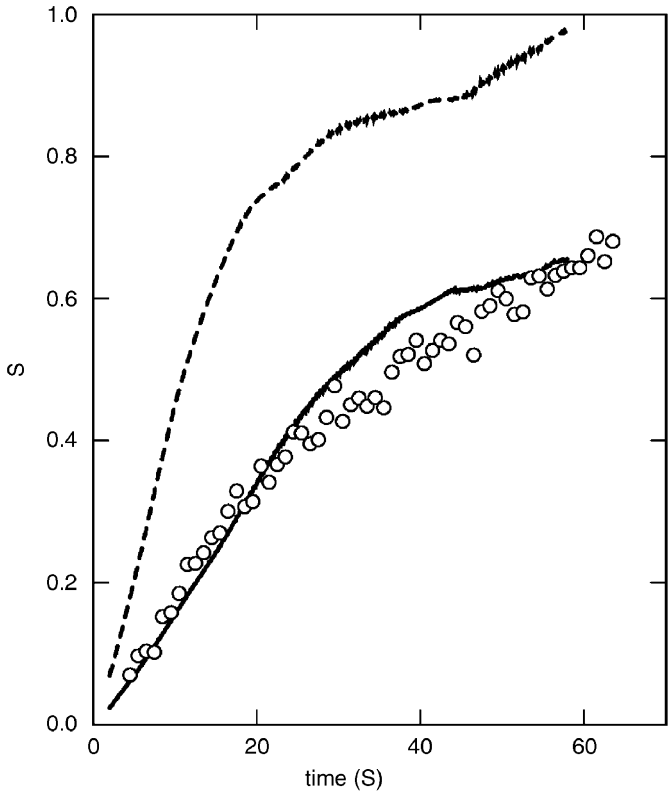

Fig. 11. Segregation rate as a function of time for a freely bubbling fluidized bed with 1.5 and 2.5 mm (diameter) particles. The lines represent the results from DPM simulations: the solid line is obtained with the drag relation for bidisperse systems, the dashed line is obtained with the standard drag model. The symbols represent the experimental result (after Beetstra et al., 2006b).

in the simulation consisted of 45,000 particles (25% small particles and 75% large particles) and the fluidization velocity is 1.30 m/s. The various other parameters in the simulations were chosen such to match the experimental conditions as close as possible. From the fraction of large and small particles in the cell, both in experiment and simulation, the degree of segregation s is determined, which is defined as:

$$s = \frac{S - 1}{S_{\max} - 1}, \tag{49}$$

where $S = \langle h_{\text{small}} \rangle / \langle h_{\text{large}} \rangle$ and $S_{\max} = (x_{\text{large}} + 1)/x_{\text{large}}$, $\langle h_i \rangle$ being the average height of particles of type i and x_{large} the volume fraction of large particles. Thus, for a completely mixed system $s = 0$, and for a completely segregated system $s = 1$. In Fig. 11 we show the segregation rate as a function of time, from the experiment (points) and from the discrete particle simulations using two different drag force relations (lines).

It can be seen that in the simulations with the standard drag correlations (in which the bidispersity is not explicitly taken into account), the system is almost completely segregated after 1 min, whereas the segregation in the experiment is only about 64% after the same period of time. The degree of segregation in the simulation with the new drag relation by Beetstra et al. (2006b) has a value of 65% after 1 min, and the rate at which the segregation occurs in the same simulation also compares very well with the trend observed in the experiment. For a more detailed description of these simulations we refer to the contribution by Beetstra et al. (2006b) in this issue.

7. Outlook

Based on the examples discussed in the preceding sections, it is evident that the DPM is a very powerful tool to study the details of flow phenomena prevailing in fluidized beds. The main reason for its success is the reliable description of the particle–particle collisions, since many processes are to a large extent determined by the collision frequency (e.g. granulation processes). Moreover, the phenomena prevailing at the level of individual particles can be naturally incorporated since the properties of each individual particle are described separately. System properties such as size and density distributions can therefore be incorporated in a straightforward fashion. Furthermore, properties such as temperature, specific area available for chemical reaction or wetness can be assigned to each individual particle. In the future three-dimensional versions of the DPM should be extended to incorporate all necessary details to model various chemical engineering problems. In this respect first attempts, mainly in two dimensions, have already been reported in literature. We will conclude this review with a few examples where these kind of problems have been investigated. Kaneko et al. (1999) who studied gas-phase olefin polymerization, including a description of the energy balance and the

chemical reaction rate at the level of individual particles. They demonstrated the effect of elevated pressure on the fluidization behavior and the heat transfer. Furthermore, they demonstrated that a non-uniform gas supply system can lead to undesirable hot spot formation in the polymerization process.

Goldschmidt et al. (2003b) used the DPM to describe fluidized bed spray granulation. To this end they considered several discrete elements, i.e. dry particles, wet particles and droplets, including rules for each possible contact of the various elements. They demonstrated that the DPM can be used to investigate the particle size distribution resulting from different nozzle configurations.

Czok et al. (2005) modeled chemical vapor deposition with the aid of a three-dimensional DPM. In their model, the formation of a thin aluminum coating on glass spheres was described through a simple growth kernel depending on the local tri-isobutyl-aluminum concentration. Their calculation revealed zones of insufficient mixing near the wall, in the corners and near the bottom plate, and zones of possible agglomeration due to excessive deposition.

Link et al. (2006) studied the granulation in spout-fluid beds with a three-dimensional DPM. They found that the growth rate scales with the projected surface area of the particle and that two growth mechanisms could be identified in the simulations, i.e. very fast growth in the nozzle region and a more modest, though constant growth outside the nozzle region. See for more information the paper by Link et al. (2006) in this issue.

Although in most of these examples only a limited number of parameters have been varied, it clearly shows the powerful capabilities of the DPM. Given the steady improvement in computational resources, it is expected that the DPM can be used to tackle various problems of increasing size (in the terms of number of particles) and complexity in the future. This will enable the researchers in the field of discrete particle modeling to generate data to improve the closure relations that are required by more coarse-grained models in the multi-level modeling approach.

Notation

a	ratio between cube diameter and particle diameter, dimensionless
C_D	drag coefficient, dimensionless
d	diameter, m
D	distribution function, dimensionless
e_n	coefficient of normal restitution, dimensionless
$\mathbf{F}_{ab}$	contact force, N
f	volume fraction, dimensionless
$\mathbf{g}$	gravitational acceleration, $\mathrm{m/s^2}$
$\langle h_i \rangle$	average height of particles of type i, m
$\mathbf{H}$	rotation matrix, dimensionless
I	moment of inertia, N m
$\mathbf{I}$	unit matrix, dimensionless
J	impulse, kg m/s
$\mathbf{J}_{ab}$	impulse vector, kg m/s
k	spring stiffness, N/m
m_{ab}	effective mass, kg
m_p	particle mass, kg
n	computational time step, dimensionless
$\mathbf{n}_{ab}$	normal unit vector, dimensionless
N	number specified by subscript, dimensionless
p	pressure, Pa
$\mathbf{r}$	position, m
r	radius, m
s	degree of segregation, dimensionless
$\mathbf{S}_p$	particle drag sink term, $\mathrm{N/m^3}$
$\mathbf{t}_{ab}$	tangential unit vector, dimensionless
t	time, s
$\mathbf{T}$	torque, N m
$\mathbf{u}_f$	fluid velocity, m/s
$\mathbf{v}_i$	velocity of particle i, m/s
$\mathbf{v}_{ab}$	relative velocity at the contact point, m/s
V	volume, $\mathrm{m^3}$
x_{large}	volume fraction of large particles, dimensionless

Greek letters

β	inter-phase momentum transfer coefficient, $\mathrm{kg/m^3 s}$
β_0	coefficient of tangential restitution, dimensionless
$\boldsymbol{\delta}$	displacement, m
ε	volume fraction, dimensionless
η	damping coefficient, N s/m
λ_f	gas phase bulk viscosity, kg/m s
μ_g	gas phase shear viscosity, kg/m s
μ	dynamic friction coefficient, dimensionless
ρ	density, $\mathrm{kg/m^3}$
$\boldsymbol{\tau}_g$	gas phase stress tensor, Pa
ϕ	general variable
$\boldsymbol{\Phi}$	flux, $\mathrm{kg/m^2\,s}$
$\boldsymbol{\omega}$	angular velocity, 1/s

Subscripts

0	prior to collision
a, b	particle indices
cell	computational grid cell
n	normal direction
p	particle
t	tangential direction

References

Andrews IV, A.T., Loezos, P.N., Sundaresan, S., 2005. Coarse-grid simulation of gas–particle flows in vertical risers. Engineering Chemistry Research 44 (16), 6022–6037.

Benyahia, S., Syamlal, M., O'Brien, T.J., 2006. Extension of Hill–Koch–Ladd drag correlation over all ranges of Reynolds number and solids volume fraction. Powder Technology 162 (2), 166–174.

Beetstra, R., Van der Hoef, M.A., Kuipers, J.A.M., 2006a. Drag force from lattice Boltzmann simulations of intermediate Reynolds number flow past mono- and bidisperse arrays of spheres. A.I.Ch.E. Journal, accepted for publication.

Beetstra, R., Van der Hoef, M.A., Kuipers, J.A.M., 2006b. Numerical study of segregation using a new drag force correlation for polydisperse systems derived from lattice Boltzmann simulations. Chemical Engineering Science, the special issue on Fluidized bed applications, accepted for publication, doi: 10.1016/j.ces.2006.08.054.

Bokkers, G.A., 2005. Multi-level modeling of the hydrodynamics in gas phase polymerisation reactors. Ph.D. Thesis, University of Twente, Enschede.

Bokkers, G.A., Van Sint Annaland, M., Kuipers, J.A.M., 2004. Mixing and segregation in a bidisperse gas–solid fluidised bed: a numerical and experimental study. Powder Technology 140 (3), 176–186.

Campbell, C.S., Brennen, C.E., 1985. Computer simulations of granular shear flows. Journal of Fluid Mechanics 151, 167–188.

Chen, C., Fan, L.-S., 2004. Discrete simulation of gas–liquid bubble columns and gas–liquid–solid fluidized beds. A.I.Ch.E. Journal 50 (2), 288–301.

Cundall, P.A., Strack, O.D.L., 1979. A discrete numerical model for granular assemblies. Geotechnique 29 (1), 47–65.

Czok, G., Kuipers, J.A.M., Ye, M., Werther, J., 2005. Modeling of chemical vapor deposition in a fluidized bed reactor based on discrete particle simulation. International Journal of Chemical Reactor Engineering 3, A57.

Dahl, S.R., Hrenya, C.M., 2004. Size segregation in rapid, granular flows with continuous size distributions. Physics of Fluids 16 (1), 1–13.

Dahl, S.R., Hrenya, C.M., 2005. Size segregation in gas–solid fluidized beds with continuous size distributions. Chemical Engineering Science 60 (23), 6658–6673.

Dahl, S.R., Clelland, R., Hrenya, C.M., 2004. The effects of continuous size distributions on the rapid flow of inelastic particles. Physics of Fluids 14 (6), 1972–1984.

Delnoij, E., Kuipers, J.A.M., Van Swaaij, W.P.M., 1999. A three-dimensional CFD model for gas–liquid bubble columns. Chemical Engineering Science 54 (13–14), 2217–2226.

Ergun, S., 1952. Fluid flow through packed columns. Chemical Engineering Progress 48, 89–94.

Feng, Y.Q., Yu, A.B., 2004. Assessment of model formulations in the discrete particle simulation of gas–solid flow. Industrial & Engineering Chemistry Research 43 (26), 8378–8390.

Feng, Y.Q., Xu, B.H., Zhang, S.J., Yu, A.B., Zulli, P., 2004. Discrete particle simulation of gas fluidization of particle mixtures. A.I.Ch.E. Journal 50 (8), 1713–1728.

Fu, J., Adams, M.J., Reynolds, G.K., Salman, A.D., Hounslow, M.J., 2004. Impact deformation and rebound of wet granules. Powder Technology 140 (3), 248–257.

Goldschmidt, M.J.V., Kuipers, J.A.M., Van Swaaij, W.P.M., 2001. Hydrodynamic modeling of dense gas-fluidised beds using the kinetic theory of granular flow: effect of coefficient of restitution on bed dynamics. Chemical Engineering Science 56 (2), 571–578.

Goldschmidt, M.J.V., Beetstra, R., Kuipers, J.A.M., 2002. Hydrodynamic modelling of dense gas-fluidised beds: comparison of the kinetic theory of granular flow with 3D hard-sphere discrete particle simulations. Chemical Engineering Science 57 (11), 2059–2075.

Goldschmidt, M.J.V., Link, J.M., Mellema, S., Kuipers, J.A.M., 2003a. Digital image analysis measurements of bed expansion and segregation dynamics in dense gas-fluidised beds. Powder Technology 138 (2–3), 135–159.

Goldschmidt, M.J.V., Weijers, G.G.C., Boerefijn, R., Kuipers, J.A.M., 2003b. Discrete element modelling of fluidised bed spray granulation. Powder Technology 138 (1), 39–45.

Goldschmidt, M.J.V., Beetstra, R., Kuipers, J.A.M., 2004. Hydrodynamic modelling of dense gas-fluidised beds: comparison and validation of 3D discrete particle and continuum models. Powder Technology 142 (1), 23–47.

He, Y., Van Sint Annaland, M., Deen, N.G., Kuipers, J.A.M., 2006. Gas–solid two-phase turbulent flow in a circulating fluidized bed riser: an experimental and numerical study, Proceedings of the Fifth World Congress on Particle Technology, April 23–27, 2006, Orlando, FL, USA.

Helland, E., Occelli, R., Tadrist, L., 1999. Numerical study of cohesive powders in a dense fluidized bed. Comptes Rendus de l'Academie de Sciences—Serie IIb: Mecanique, Physique, Chimie, Astronomie 327 (14), 1397–1403.

Helland, E., Occelli, R., Tadrist, L., 2000. Numerical study of cluster formation in a gas–particle circulating fluidized bed. Powder Technology 110 (3), 210–221.

Helland, E., Occelli, R., Tadrist, L., 2002. Computational study of fluctuating motions and cluster structures in gas–particle flows. International Journal of Multiphase Flow 28 (2), 199–223.

Helland, E., Occelli, R., Tadrist, L., 2005. Numerical study of cluster and particle rebound effects in a circulating fluidised bed. Chemical Engineering Science 60 (1), 27–40.

Hill, R.J., Koch, D.L., Ladd, J.C., 2001. Moderate-Reynolds-numbers flows in ordered and random arrays of spheres. Journal of Fluid Mechanics 448, 243–278.

Hoomans, B.P.B., Kuipers, J.A.M., Briels, W.J., Van Swaaij, W.P.M., 1996. Discrete particle simulation of bubble and slug formation in a two-dimensional gas-fluidised bed: a hard-sphere approach. Chemical Engineering Science 51 (1), 99–118.

Hoomans, B.P.B., Kuipers, J.A.M., Van Swaaij, W.P.M., 2000. Granular dynamics simulation of segregation phenomena in bubbling gas-fluidised beds. Powder Technology 109 (1–3), 41–48.

Hoomans, B.P.B., Kuipers, J.A.M., Mohd Salleh, M.A., Stein, M., Seville, J.P.K., 2001. Experimental validation of granular dynamics simulations of gas-fluidised beds with homogenous in-flow conditions using positron emission particle tracking. Powder Technology 116 (2–3), 166–177.

Ibsen, C.H., 2002. An experimental and computational study of gas–particle flow in circulating fluidised reactors. Ph.D. Thesis, Aalborg University Esbjerg, Denmark.

Ibsen, C.H., Helland, E., Hjertager, B.H., Solberg, T., Tadrist, L., Occelli, R., 2004. Comparison of multifluid and discrete particle modelling in numerical predictions of gas particle flow in circulating fluidised beds. Powder Technology 149 (1), 29–41.

Iwadate, M., Horio, M., 1998. Agglomerating fluidization of wet powders and group C powders: a numerical analysis. In: Fan, L.S., Knowlton, T. (Eds.), Fluidization IX. Engineering Foundation, Durango, USA, p. 293.

Jenkins, J.T., Savage, S.B., 1983. Theory for the rapid flow of identical, smooth, nearly elastic, spherical particles. Journal of Fluid Mechanics 130, 187–202.

Johnson, K.L., 1985. Contact Mechanics. Cambridge University Press, Cambridge, UK.

Kafui, K.D., Thornton, C., Adams, M.J., 2002. Discrete particle-continuum fluid modelling of gas–solid fluidised beds. Chemical Engineering Science 57 (12), 2395–2410.

Kaneko, Y., Shiojima, T., Horio, M., 1999. DEM simulation of fluidized beds for gas-phase olefin polymerization. Chemical Engineering Science 54 (24), 5809–5821.

Kharaz, A.H., Gorham, D.A., Salman, A.D., 1999. Accurate measurement of particle impact parameters. Measurement Science and Technology 10, 31–35.

Kawaguchi, T., Tanaka, T., Tsuji, Y., 1998. Numerical simulation of two-dimensional fluidized beds using the discrete element method (comparison between the two- and three-dimensional models). Powder Technology 96 (2), 129–138.

Kuwagi, K., Mikami, T., Horio, M., 2000. Numerical simulation of metallic solid bridging particles in a fluidized bed at high temperature. Powder Technology 109 (1–3), 27–40.

Langston, P.A., Tüzün, U., Heyes, D.M., 1994. Continuous potential discrete particle simulations of stress and velocity fields in hoppers transition from fluid to granular flow. Chemical Engineering Science 49 (8), 1259–1275.

Li, J., Kuipers, J.A.M., 2002. Effect of pressure on gas–solid flow behavior in dense gas-fluidized beds: a discrete particle simulation study. Powder Technology 127 (2), 173–184.

Li, J., Kuipers, J.A.M., 2003. Gas–particle interactions in dense gas-fluidized beds. Chemical Engineering Science 58 (3–6), 711–718.

Li, J., Kuipers, J.A.M., 2005. On the origin of heterogeneous structure in dense gas–solid flows. Chemical Engineering Science 60 (5), 1251–1265.

Li, Y., Zhang, J., Fan, L.-S., 1999. Numerical simulation of gas–liquid–solid fluidization systems using a combined CFD-VOF-DPM method: bubble wake behavior. Chemical Engineering Science 54 (21), 5101–5107.

Li, Y., Yang, G.Q., Zhang, J.P., Fan, L.-S., 2001. Numerical studies of bubble formation dynamics in gas–liquid–solid fluidization at high pressures. Powder Technology 116 (2–3), 246–260.

Limtrakul, S., Boonsrirat, A., Vatanatham, T., 2004. DEM modeling and simulation of a catalytic gas–solid fluidized bed reactor: a spouted bed as a case study. Chemical Engineering Science 59 (22–23), 5225–5231.

Link, J., Zeilstra, C., Deen, N., Kuipers, H., 2004. Validation of a discrete particle model in a 2D spout-fluid bed using non-intrusive optical

measuring techniques. Canadian Journal of Chemical Engineering 82 (1), 30–36.

Link, J.M., Cuypers, L.A., Deen, N.G., Kuipers, J.A.M., 2005. Flow regimes in a spout-fluid bed: a combined experimental and simulation study. Chemical Engineering Science 60 (13), 3425–3442.

Link, J.M., Godlieb, W., Deen, N.G., Kuipers, J.A.M., 2006. Discrete element study of granulation in a spout-fluidized bed. Chemical Engineering Science, the special issue on Fluidized bed applications, accepted for publication, doi: 10.1016/j.ces.2006.08.018.

Lu, H., Wang, S., Zhao, Y., Yang, L., Gidaspow, D., Ding, J., 2005. Prediction of particle motion in a two-dimensional bubbling fluidized bed using discrete hard-sphere model. Chemical Engineering Science 60 (13), 3217–3231.

Lun, C.C.K., 2000. Numerical simulation of dilute turbulent gas–solid flows. International Journal of Multiphase Flow 26, 1707–1736.

McNamara, S., Young, W.R., 1992. Inelastic collapse and clumping in a one-dimensional granular medium. Physics of Fluids 4 (3), 496–504.

Mikami, T., Kamiya, H., Horio, M., 1998. Numerical simulation of cohesive powder behavior in a fluidized bed. Chemical Engineering Science 53 (10), 1927–1940.

Ouyang, J., Li, J., 1999a. Particle-motion-resolved discrete model for simulating gas–solid fluidization. Chemical Engineering Science 54 (13–14), 2077–2083.

Ouyang, J., Li, J., 1999b. Discrete simulations of heterogeneous structure and dynamic behavior in gas–solid fluidization. Chemical Engineering Science 54 (22), 5427–5440.

Pandit, J.K., Wang, X.S., Rhodes, M.J., 2005. Study of Geldart's group A behaviour using the discrete element method simulation. Powder Technology 160 (1), 7–14.

Potic, B., Kersten, S.R.A., Ye, M., Van der Hoef, M.A., Kuipers, J.A.M., Van Swaaij, W.P.M., 2005. Fluidization with hot compressed water in micro-reactors. Chemical Engineering Science 60, 5982–5990.

Rhodes, M.J., Wang, X.S., Nguyen, M., Stewart, P., Liffman, K., 2001a. Study of mixing in gas-fluidized beds using a DEM model. Chemical Engineering Science 56 (8), 2859–2866.

Rhodes, M.J., Wang, X.S., Nguyen, M., Stewart, P., Liffman, K., 2001b. Use of discrete element method simulation in studying fluidization characteristics: influence of interparticle force. Chemical Engineering Science 56 (1), 69–76.

Ristow, G.H., 2000. Pattern Formation in Granular Materials. Springer, New York.

Schäfer, J., Dippel, S., Wolf, D.E., 1996. Force schemes in simulations of granular materials. Journal de Physique I 6 (1), 5–20.

Takeuchi, S., Wang, S., Rhodes, M., 2004. Discrete element simulation of a flat-bottomed spouted bed in the 3-D cylindrical coordinate system. Chemical Engineering Science 59 (17), 3495–3504.

Takeuchi, S., Wang, X.S., Rhodes, M.J., 2005. Discrete element study of particle circulation in a 3-D spouted bed. Chemical Engineering Science 60 (5), 1267–1276.

Tsuji, Y., Kawaguchi, T., Tanaka, T., 1993. Discrete particle simulation of two-dimensional fluidized bed. Powder Technology 77 (1), 79–87.

Van der Hoef, M.A., Van Sint Annaland, M., Kuipers, J.A.M., 2004. Computational fluid dynamics for dense gas–solid fluidized beds: a multi-scale modeling strategy. Chemical Engineering Science 59 (22–23), 5157–5165.

Van der Hoef, M.A., Van Sint Annaland, M., Kuipers, J.A.M., 2005. Computational fluid dynamics for dense gas–solid fluidized beds: a multi-scale modeling strategy. China Particuology 3 (1–2), 69–77.

Van der Hoef, M.A., Ye, M., Van Sint Annaland, M., Andrews IV, A.T., Sundaresan, S., Kuipers, J.A.M., 2006. Multi-scale modeling of gas-fluidized beds. In: Advances in Chemical Engineering, vol. 31, pp. 65.

Van Sint Annaland, M., Deen, N.G., Kuipers, J.A.M., 2005. Numerical simulation of gas–liquid–solid flows using a combined front tracking and discrete particle method. Chemical Engineering Science 60 (22), 6188–6198.

Van Wachem, B.G.M., Schouten, J.C., Van den Bleek, C.M., Krishna, R., Sinclair, J.L., 2001. Comparative analysis of CFD models of dense gas–solid systems. A.I.Ch.E. Journal 47 (5), 1035–1051.

Vreman, A.W., Al-Tarazi, M., Kuipers, J.A.M., Van Sint Annaland, M., Bokhove, O., 2006. Rapid shallow granular and hydraulic flow through a contraction. Journal of Fluid Mechanics, submitted for publication.

Walton, O.R., Braun, R.L., 1986. Viscosity and temperature calculations for assemblies of inelastic frictional disks. Journal of Rheology 30 (5), 949–980.

Wang, X.S., Rhodes, M.J., 2003. Determination of particle residence time at the walls of gas fluidized beds by discrete element method simulation. Chemical Engineering Science 58 (2), 387–395.

Wang, X.S., Rhodes, M.J., 2004a. Mechanistic study of defluidization by numerical simulation. Chemical Engineering Science 59 (1), 215–222.

Wang, X.S., Rhodes, M.J., 2004b. Numerical study of gas fluidization under increased 'gravity'. Advanced Powder Technology 15 (6), 629–638.

Wang, X.S., Rhodes, M.J., 2005a. A DEM study of particle motion near the walls of gas fluidized beds. Powder Technology 160 (1), 15–19.

Wang, X.S., Rhodes, M.J., 2005b. Pulsed fluidization—a DEM study of a fascinating phenomenon. Powder Technology 159 (3), 142–149.

Wang, X.S., Rhodes, M.J., 2005c. Using pulsed flow to overcome defluidization. Chemical Engineering Science 60 (18), 5177–5181.

Wen, Y.C. Yu, Y.H., 1966. Mechanics of Fluidization. Chemical Engineering Progress Symposium Series, vol. 62, pp. 100–111.

Xu, B.H., Yu, A.B., 1997. Numerical simulation of the gas–solid flow in a fluidized bed by combining discrete particle method with computational fluid dynamics. Chemical Engineering Science 52 (16), 2785–2809.

Xu, B.H., Yu, A.B., Chew, S.J., Zulli, P., 2000. Numerical simulation of the gas–solid flow in a bed with lateral gas blasting. Powder Technology 109 (1–3), 13–26.

Ye, M., Van der Hoef, M.A., Kuipers, J.A.M., 2004. A numerical study of fluidization behavior of Geldart A particles using a discrete particle model. Powder Technology 139 (2), 129–139.

Ye, M., Van der Hoef, M.A., Kuipers, J.A.M., 2005a. From discrete particle model to a continuous model of Geldart A particles. Chemical Engineering Research and Design 83 (7A), 833–843.

Ye, M., Van der Hoef, M.A., Kuipers, J.A.M., 2005b. The effects of particle and gas properties on the fluidization of Geldart A particles. Chemical Engineering Science 60 (16), 4567–4580.

Yu, A.B., Xu, B.H., 2003. Particle-scale modelling of gas–solid flow in fluidisation. Journal of Chemical Technology and Biotechnology 78 (2–3), 111–121.

Zhang, J., Fan, L.-S., Zhu, C., Pfeffer, R., Qi, D., 1999. Dynamic behavior of collision of elastic spheres in viscous fluids. Powder Technology 106 (1–2), 98–109.

Zhang, J., Li, Y., Fan, L.-S., 2000a. Numerical studies of bubble and particle dynamics in a three-phase fluidized bed at elevated pressures. Powder Technology 112 (1–2), 46–56.

Zhang, J., Li, Y., Fan, L.-S., 2000b. Discrete phase simulation of gas–liquid–solid fluidization systems: single bubble rising behavior. Powder Technology 113 (3), 310–326.

Zhou, H., Flamant, G., Gauthier, D., Lu, J., 2004. Numerical simulation of the turbulent gas–particle flow in a fluidized bed by an LES-DPM model. Chemical Engineering Research and Design 82 (A7), 918–926.